Nanostructured TiO_2/CuO Dual-coated Copper Meshes with Superhydrophilic, Underwater Superoleophobic and Self-Cleaning Properties for Highly Efficient Oil/Water Separation

Shaojun Yuan, Chen Chen, Aikifa Raza, Ruixue Song, Tie-Jun Zhang, Simo O. Pehkonen, Bin Liang

PII: S1385-8947(17)31223-8
DOI: http://dx.doi.org/10.1016/j.cej.2017.07.075
Reference: CEJ 17341

To appear in: *Chemical Engineering Journal*

Received Date: 23 April 2017
Revised Date: 7 July 2017
Accepted Date: 12 July 2017

Please cite this article as: S. Yuan, C. Chen, A. Raza, R. Song, T-J. Zhang, S.O. Pehkonen, B. Liang, Nanostructured TiO_2/CuO Dual-coated Copper Meshes with Superhydrophilic, Underwater Superoleophobic and Self-Cleaning Properties for Highly Efficient Oil/Water Separation, *Chemical Engineering Journal* (2017), doi: http://dx.doi.org/10.1016/j.cej.2017.07.075

Nanostructured TiO_2/CuO Dual-coated Copper Meshes with Superhydrophilic, Underwater Superoleophobic and Self-Cleaning Properties for Highly Efficient Oil/Water Separation

Shaojun Yuan,[a,*] Chen Chen,[a] Aikifa Raza,[b] Ruixue Song,[a] Tie-Jun Zhang,[b] Simo O. Pehkonen,[c] Bin Liang[a]

[a]Multi-phase Mass Transfer & Reaction Engineering Lab,
College of Chemical Engineering,
Sichuan University, Chengdu 610065, China
[b] Department of Mechanical and Materials Engineering,
Masdar Institute of Science and Technology,
P.O. Box 54224, Abu Dhabi, UAE
[c] Department of Environmental and Biosciences,
University of Eastern Finland, 70211 Kuopio, Finland.

*To whom all correspondence should be addressed
Tel: +86-28-85990133, Fax: +86-28-85460556
E-mail: yuanshaojun@gmail.com (S.J. Yuan)

Abstract

Oil-contaminated water caused by either oil spill disasters or industrial disposal has posed a global risk to environmental sustainability and human health. To address the ever-growing need for highly efficient separation of oil/water mixtures, nanostructured TiO_2/CuO dual coatings were fabricated on the copper mesh by a combination of electrochemical anodization and layer-by-layer self-assembly deposition to render its surface with superhydrophilic, underwater superoleophobic and self-cleaning functionality. $Cu(OH)_2$ nanoneedle arrays (NNA) were vertically grown from the copper mesh surfaces by electrochemical anodization processes, followed by the deposition of TiO_2 multilayer on the $Cu(OH)_2$ NNA via layer-by-layer assembly prior to being calcinated to form TiO_2/CuO dual coatings. The nanostructured TiO_2/CuO NNA dual-coated copper meshes were demonstrated to exhibit a high separation efficiency (oil residue content less than 20 ppm), excellent water flux (more than 80 $kL \cdot h^{-1} \cdot m^{-2}$), and desirable self-cleaning ability under ultraviolet (UV) illumination. The photo-catalytic ability of the deposited TiO_2 layers enabled the facile and rapid removal of the oil contaminants on the mesh surface under UV illumination to recover oil/water separation ability of the as-fabricated mesh for recycle use. With the adherent features of superhydrophilicity, underwater superoleophobicity and self-cleaning ability, the proposed TiO_2/CuO NNA dual-coated meshes are potentially useful in practical oil/water separation applications.

***Keyword*:** Oil/water separation, nanostructured TiO_2/CuO dual coatings, self-cleaning, copper mesh, underwater superoleophobicity

1. Introduction

With the frequent occurrence of oil spill accidents during offshore oil production and transportation and the increasing release of oily industrial wastewater, as well as the resulting tougher regulation regarding oily industrial wastewater discharge, oil/water separation has become a global challenge for the protection of environmental sustainability and aqueous ecosystems [1]. Various strategies, such as oil skimmers [2], air flotation [3], gravity separation [4], oil-absorbing materials [5], coagulation [6] and flocculation and coalescence [7], have been proposed to accomplish oil/water separation for the mitigation of environmental damage by oily wastewater. However, these conventional methods are limited by their low separation efficiency, high energy consumption, complex separation process and secondary pollution [8]. It is, therefore, of great importance to develop an alternative highly efficient and low-cost approach to address the ever-growing need for oily wastewater treatment.

Due to different interfacial effect of oil and water, advanced materials with preferential wettability towards oil or water are considered to be more effective and more advantageous alternative approach for overcoming this knotty issue over last decades. Various superwetting materials with superhydrophobic or superoleophobic surfaces, fabricated by chemical etching [9, 10], electro-spinning [11, 12], chemical vapor deposition [13], graft polymerization [14], self-assembly [15, 16], and hydrothermal synthesis [17], have been extensively employed in industrial oily wastewater treatment. These superwetting materials are generally classified into oil-loving and water-loving materials [18]. It has been widely recognized that the oil-loving (i.e. superhydrophobic-superoleophilic) materials are readily subject to some intractable problems, such as easy fouling or even blocking up by oils, quick

decline of permeation owing to oil adsorption and pore plugging by oil droplets, difficulty in cleaning and recycling, and secondary contamination to environments during the post-treatment process [19]. On the contrary, water-loving (i.e. superhydrophilic and underwater superoleophobic) materials have been demonstrated advantages of high separation efficiency and filtration flux, low oil fouling, and easy recycle for oil/water separation in recent years, hence they have gained considerable attention as novel superwetting materials to replace of oil-loving type of materials.

As the wettability of a solid surface is governed by chemical compositions and geometrical structures, superhydrophilic and underwater superoleophobic materials are generally fabricated by creating hierarchical micro/nano-structures on hydrophilic substrates [20], or by surface modification of an appropriate rough surface with hydrophilic materials. Surface modification of metal meshes can be accomplished by either grafting of hydrophilic polymer coatings or deposition of inorganic materials coatings [20-22]. The hydrophilic polymeric coatings grafted on the metal meshes are found susceptible to degradation or swelling behaviors under harsh environments, Meanwhile, inorganic material coatings formed on metal mesh by hydrothermal-based synthesis [17, 23, 24] or electro-deposition [25-27] are virtually not suitable for practical applications, because of difficulty in large-scale production, toxic or expensive reagents, and uncontrollable geometric structures [20]. In contrast, electrochemical anodization provides a promising alternative approach to produce well-ordered nanostructures over large areas due to the featured advantages of simple operation, low cost, and easy scale-up for practical applications [28]. Although this methodology has been reported to be liable to cause damage of substrates [29], its noticeable advantages is to precisely control surface morphology and thickness of oxide films by varying electrolytes, current density, temperature and reaction time. In the mean time, the adhesion of anodic oxide film on copper meshes has also been found more stable and robust than that of most types of oxide layers by chemical

etching [30], which make them less likely to crack and to peel from aging and wear. However, to the best our knowledge, few studies have been documented to fabricate superwetting metal meshes using electrochemical anodization for oil/water separation.

The main concern of hydrophilic or superhydrophilic separation materials in oil/water separation application is that they are readily susceptible to contamination by low surface-energy substance such as oil owing to their intrinsically high surface energy [31]. Once adsorbed, these low surface-energy oils are difficult to remove or dislodge, and cause the loss of wetting behaviors of these separation materials, thus resulting in the substantial decrease in their separation efficiency of oil/water mixtures. Enlightened by the excellent of optical and photo-catalytic properties of TiO_2 particles, self-cleaning metal meshes have been recently reported to circumvent the intractable contamination problem of the separation mesh [23]. Zhang et al. [32] fabricated underwater superoleophobic and self-cleaning silicate/TiO_2 dual-coated stainless steel meshes by layer-by-layer self-assembly, and demonstrated decomposition of organic contaminants by TiO_2-induced photo-catalysis under UV illumination. Liu et al. [33] fabricated underwater oleophobic nanostructured TiO_2-coated copper meshes by combination of chemical etching and hydrothermal synthesis for highly efficient oil/water separation and self-cleaning under solar light illumination. Du et al. [34] demonstrated switchable and simultaneous oil/water separation on a TiO_2-coated stainless steel mesh with superamphiphilic self-cleaning property. Song et al. reported an underwater superoleophobic $BiVO_4$-coated mesh with sunlight-induced self-cleaning property for oil/water separation application. Taken together, deposition of photocatalyst nanoparticles, especially for TiO_2, on the nanostructured surfaces is usually utilized to render superwetting metal meshes with self-cleaning capability for recycle use in an oil/water separation process. However, few studies have been

documented to deposit TiO_2 on anodization-derived nanostructures for oil/water separation.

Accordingly, the purpose of this study is to fabricate self-cleaning underwater superoleophobic nanostructured TiO_2/CuO dual-coated copper meshes by the combination of electrochemical anodization and layer-by-layer (LBL) self-assembly deposition for highly efficient oil/water separation. As schematically illustrated in Figure 1, $Cu(OH)_2$ nanoneedle arrays (NNA) were first fabricated on the surfaces of copper meshes by electrochemical anodization, followed by deposition of TiO_2 multilayer by using LBL self-assembly onto the $Cu(OH)_2$ NNA coatings, and finally calcinated to form TiO_2/CuO dual-coated copper meshes. Success in each fabrication step was ascertained by scanning electron microscopy (SEM) and energy dispersive X-ray spectroscopy (EDS), X-ray diffraction (XRD), X-ray photoelectron spectroscopy (XPS), dynamic water contact angle and underwater oil contact angle measurements. The as-fabricated TiO_2/CuO NNA dual-coated copper meshes were investigated to determine their separation efficiency and water flux of various oil/water mixture, and to evaluate the self-cleaning ability towards contaminated copper meshes under UV illustration. With the inherent good stability and durability, high separation efficiency and self-cleaning ability of the metal meshes, the current methodology potentially contributes to the development of advanced superwetting materials for practical oil/water separation applications.

2. Experimental

2.1 Materials.

Copper meshes (99.9%, wire thickness 50 μm, 200 meshes) were purchased from Anping Shengzhuo Metal Wire Mesh Co. (Hebei, China). All of the reagent-grade chemical reagents, such as KOH, NH_4Cl, NH_4F, and red oil, and organic solvents, such as ethanol, isopropyl alcohol, acetone and toluene, were obtained from Kelong Chem. Co. (Chengdu, China) and were all used as received. Titanium butoxide, olive oil, dichloromethane, n-hexane, and isooctane were all purchased from Sigma-Aldrich Chemical Co. (St. Louis, MO) and used as received. Kerosene and crude oil were kindly provided by an oil company located at Abu Dhabi (UAE). Chemical oxygen demand (COD) measurement reagents, such as $K_2Cr_2O_7$, H_2SO_4 (98%), $HgSO_4$, Ag_2SO_4, and $(NH_4)_2Fe(SO_4)_2 \cdot 6H_2O$, were obtained from Aladdin Industrial Co. (Shanghai, China). Ultrapure deionized water from an Ulupure-II-20T water system (Chengdu, China) was used throughout the whole experiments.

2.2 Preparation of $Cu(OH)_2$ nanoneedle arrays on the copper meshes.

The copper meshes were trimmed into the dimensions of 8 cm in length and 6 cm in width, followed by ultrasonically degreasing in acetone, isopropyl alcohol, ethanol and deionized water, in that order for 15 min each, and were finally immersed in a 2 mol L^{-1} HCl aqueous solution for 30 min to remove the oxide layer to obtain a clean and oxide-free surface of copper mesh. The preparation of $Cu(OH)_2$ nanoneedle arrays (NNA) films were accomplished by electrochemical anodization using a similar procedure as described in our previous studies [30]. Briefly, the pretreated copper mesh was used as working (anode) electrode with a surface area of 36 cm^2 (three quarters of the copper mesh immersed in the electrolyte solution), and a platinum (Pt) foil as the counter (cathode) electrode with the same area. The copper anode and Pt cathode were fixed in a Teflon electrolytic cell with a distance of 2 cm

and connected to a direct-current power supply (HAP 03-100, Huatai Co., China). The anodization reaction was allowed to proceed at a temperature of 10^{o}C, which was maintained by placing the electrolytic cell in a cryogenic thermostatic bath, with a constant current density of 2 mA·cm^{-2} for 30 min to grow $Cu(OH)_2$ NNA films. Three types of electrolyte solutions, such as 1 mol·L^{-1} of KOH, the mixture of 1 mol·L^{-1} of KOH and 0.5 mol·L^{-1} of NH_4Cl, and the mixture of 1 mol·L^{-1} KOH and 0.5 mol·L^{-1} NH_4F, were used to determine the effect of halides on the surface features of $Cu(OH)_2$ NNA films. The appearance of a faint-blue film indicated the successful growth of $Cu(OH)_2$ NNA on the copper mesh. After electrochemical anodization treatment, the resultant copper meshes were washed with copious amounts of deionized water and dried by N_2 stream prior to being stored in a vacuum desiccator.

2.3 Formation of nanostructured TiO_2/CuO NNA dual-coated copper mesh.

The deposition of TiO_2 multilayer onto the $Cu(OH)_2$ NNA-coated meshes was achieved by our previously-proposed LBL self-assembly sol-gel method [35]. Briefly, the $Cu(OH)_2$ NNA-coated meshes were immersed in a toluene and ethanol mixture (v:v, 1:1) containing 0.1 mol·L^{-1} of titanium butoxide ($Ti(OBu)_4$) for 10 min in a sealed beaker. $Ti(OBu)_4$ can reacted readily with the hydroxyl groups on the $Cu(OH)_2$ NNA-coated mesh surfaces during this process. After the reaction, the resultant mesh was rinsed with copious amounts of toluene to remove the physically adsorbed alkoxide, if any, followed by immersing in deionized water for 2 min to regenerate the hydroxyl groups, and was finally dried by blowing pure N_2 stream. The above LBL self assembling, washing, hydrolysis and drying steps were repeated for a predetermined cycle (such as 5, 10 and 15 times) to produce the nanostructured multilayer of TiO_2/$Ti(OBu)_4$ on the $Cu(OH)_2$ NNA-coated mesh surface.

The transformation of amorphous TiO_2/$Cu(OH)_2$ NNA into crystalline TiO_2/CuO

dual coatings can be readily accomplished by calcination treatment. Typically, the as-synthesized $TiO_2/Cu(OH)_2$ NNA dual-coated copper meshes were calcined in a muffle furnace at 550 ^oC for 6 h to allow for crystallization under N_2 protection. The $Cu(OH)_2$ NNA was transformed to thermodynamically-stable CuO NNA, whilst amorphous TiO_2 multilayer were transformed anatase TiO_2, and thus resulting in the formation of nanostructured TiO_2/CuO dual-coated copper mesh. The resultant TiO_2/CuO dual-coated copper meshes obtained by 5, 10 and 15 times of LBL self assembling were defined as TiO_2*5 LBL/CuO NNA, TiO_2*10 LBL/CuO NNA, and TiO_2*15 LBL/CuO NNA dual-coated copper meshes, respectively.

2.4 Surface characterization.

The surface morphologies of the $Cu(OH)_2$ NNA-coated copper meshes obtained in different electrolytic solutions and TiO_2/CuO NNA dual-coated copper meshes obtained from different repetitions of LBL self-assembly were characterized by SEM imaging on a FEI Quanta 250 SEM (Hillsboro, Oregon, USA), together with recording EDS spectra to confirm the successful formation of nanostructured coatings. The chemical compositions of the TiO_2*15 LBL/CuO NNA dual-coated copper meshes were further characterized by XPS on a VG Microlab MKII XPS spectrometer (VG Scientific, East Grinstead, UK) with a monochromatic Al Ka X-ray source (1486.6 eV photons) using procedures described in detail previously [36]. XRD patterns of the CuO NNA and TiO_2/CuO NNA were examined by an X-ray diffractometer DX 2700 model (Haoyuan Instruments Co., Dandong, China) with Cu Kα radiation (λ = 1.5418 Å) to ascertain the crystalline structures. The UV-visible spectra and Tauc plot of the TiO_2*15 LBL/CuO NNA dual-coated copper meshes were measured by a UV-VIS-NIR spectrophotometer (UV3600, Shimadzu Co. Japan). The measurements of water contact angle (WCA) (3 μL) and oil contact angle (OCA) (3 μL) were performed on a contact angle goniometer (DM-501, Kyowa Interface

Science Co., Saitama, Japan). An average contact angle value was obtained by measuring the same meshes at three different positions.

2.5 Oil/water separation experiments.

The oil/water separation performance of the TiO_2*15 LBL/CuO NNA dual-coated copper meshes was determined by the gravity-driven oil/water mixture separation experiments. Oil/water mixture was prepared by mixing water and kerosene in a volume ratio of 1:1 (v:v), and was used for the separation experiments. For convenience, oil was stained red using oil red. Other low and high density oil/water mixtures, including hexane/water, isooctane/water and olive oil/water, were also used for separation experiments. Typically, the as-prepared copper mesh was fixed between two glass vessels with a diameter of 39 mm. After the mesh was pre-wetted by deionized water, an aliquot 2000 mL of oil/water mixture was poured onto the copper meshes, and the separation was achieved by water rapidly flowing the mesh and oil being intercepted to retain above the mesh. The whole separation process was driven solely by gravity and ended in several seconds. The filtrate water was collected and the residual oil content in the filtrate was determined by measuring COD on a COD-571 spectrophotometer (INESA Scientific Instrument Co., Shanghai, China). The conventional potassium dichromate method was adopted to determine the COD values of the residual oil in filtrate water. The separation experiments on the TiO_2*15 LBL/CuO NNA dual-coated copper meshes was repeated for at least three times until the COD values underwent a dramatic increase. Detailed procedures in the COD measurement were described in the Electric Supplementary Information (ESI S1).

The water flux of the as-fabricated copper meshes was calculated from the volume of the permeation in unit time using the following equations:

$$Flux = \frac{V}{A \cdot t} \quad (1)$$

Where V is the volume of the permeation (kL), A is the effective filtration area of the copper meshes (m^2), and t is the filtration time (h). The optical images and video of the oil/water separation process were also recorded to ascertain qualitatively the separation ability of copper meshes.

2.6 The self-cleaning and stability of the TiO_2/CuO NNA dual-coated mesh.

To ascertain the self-cleaning ability of the TiO_2/CuO NNA dual-coated copper meshes, the TiO_2*15 LBL/CuO NNA dual-coated copper meshes were contaminated by continuously performing kerosene/water separation until the COD values in filtrate water underwent a dramatic increase. Then, the contaminated meshes were washed by deionized water and dried by blowing pure N_2 stream prior to the water contact angle measurement. The kerosene-contaminated meshes were finally subject to UV illumination on a photochemical reactor equipped with a 500 W mercury light (CEL-LAM500, CEAULIGHT, Beijing, China) for a predetermined time, and the water contact angles in air were measured at predetermined intervals to evaluate the self-cleaning ability of the coated meshes, as well as to determine the optimal exposure time. The regenerated copper meshes were reused for the oil/water separation experiments, and the COD values in filtrate water were measured to assess the oil/water separation efficiency and the ability of recycle usage. In addition, the change in water contact angle and underwater oil contact angle of the coated copper meshes were recorded as a function of exposure time in deionized water to evaluate the stability and durability of the nanostructured TiO_2/CuO NNA dual-coated copper meshes.

3. Results and Discussion

3.1 SEM images of $Cu(OH)_2$ NNA surface.

The formation mechanism of $Cu(OH)_2$ nanoneedle arrays via well-established electrochemical anodization in the KOH and KOH-halide mixture electrolytes has been described in the Supplementary Information (ESI, S2.1). Figure 2 shows the respective SEM images at different magnifications for the $Cu(OH)_2$ NNA-coated copper meshes obtained from electrochemical anodization in different electrolytes. The halide ion additives have an evident effect on the growth of $Cu(OH)_2$ NNA films on the surfaces of copper meshes in their dimension, number density of nanoneedles, and nanostructure features. After being anodized in the KOH electrolyte, the surfaces of copper meshes are covered with dense and compact pine-needle-like $Cu(OH)_2$ NNA films (Figs. 2a1 and a2). The length of the $Cu(OH)_2$ nanoneedle is circa 6-10 μm, and the sharp tips of the nanoneedles are circa 160 ± 50 μm in average diameters (Fig. 2a3). This result is consistent with the fact that $Cu(OH)_2$ NNA films are successful formed on the copper mesh surfaces, as compared to the relative smooth surfaces of the pretreated copper meshes before anodization treatment (ESI, Figs. S1). However, the anodized copper meshes obtained in the KOH and halide salt mixture show a more compact surface (Figs. 2b1 and 2c1), and the Cu(OH) nanoneedles seem to be more meticulous and tenuous than those fabricated in the KOH solution (Figs. 2b2 and 2c2). In the presence of Cl^- ions, the as-synthesized $Cu(OH)_2$ nanoneedles are circa 10–15 mm in length and 90 ± 25 nm in the average diameters of the sharp tips (Fig. 2b3), whilst the $Cu(OH)_2$ nanoneedles obtained in the presence of F^- ions are circa 11-15 mm in length and 85 ± 20 nm in the average diameters of the sharp tips (Fig. 2c3). The longer and more tenuous $Cu(OH)_2$ NNA films obtained in the presence of halide Cl^- and F^- ions results in a rougher surface and larger specific surface area of the copper meshes. To further ascertain the formation of $Cu(OH)_2$ nanoneedles on the

copper meshes, EDS spectrum was recorded on the $Cu(OH)_2$ NNA-coated copper meshes obtained in the mixture electrolyte of KOH and NH_4Cl (ESI, Fig. S2a). The relative atomic ratio of [O]/[Cu] (calculated from 66.0:34.0) at circa 1.94:1 is in good agreement with the theoretical values of 2.0:1 for the $Cu(OH)_2$ species. Thereby, well-defined $Cu(OH)_2$ NNA films are grown from the copper mesh surfaces to cater for the establishment of surface superhydrophilicity as well as further modification. In this study, the $Cu(OH)_2$ NNA-coated copper meshes derived from the mixture electrolyte of KOH and NH_4Cl are chosen as the representative substrates for the subsequent deposition of TiO_2 layers.

3.2 Surface characterization of TiO_2/CuO NNA dual-coated copper mesh.

The deposition of TiO_2 multilayer onto the surfaces of $Cu(OH)_2$ NNA-coated copper meshes was accomplished by a layer-by-layer (LBL) self-assembly sol-gel process, as schematically illustrated in inset of Fig. 1. The abundant hydroxyl groups (-OH) on the $Cu(OH)_2$ NNA-coated copper mesh surfaces provide anchoring sites to bind $Ti(OBu)_4$ via self-assembly. Subsequent hydrolysis of $Ti(OBu)_4$ takes place to form $Ti(OH)_4$ layer on the $Cu(OH)_2$ NNA-coated copper meshes. These above chemisorptions and hydrolysis process are allowed to repeat for predetermined times to construct multilayer of amorphous TiO_2 nanoparticles on the $Cu(OH)_2$ NNA film. The amorphous TiO_2 and $Cu(OH)_2$ coatings are further converted into anatase TiO_2 and crystalline CuO, respectively, by calcinations or sintering process to obtain the desirable photo-catalytic ability. Our previous study has demonstrated that the NNA morphology and shape remained unchanged during the transformation of $Cu(OH)_2$ into CuO by annealing dehydration treatment [30]. Thus, the nanostructured TiO_2/CuO NNA dual-coated copper meshes with desirable superhydrophilicity, underwater superoleophobicity and self-cleaning ability have been successfully fabricated. Detailed characterization of the as-fabricated copper meshes by SEM-EDX,

XRD and XPS are discussed below.

*3.2.1 SEM imaging and EDS spectra***.**

The change in surface morphology as a function of LBL-deposited TiO_2 layers was determined by SEM imaging. Fig. 3 shows the representative SEM images at different magnifications for the TiO_2/CuO NNA dual-coated copper meshes with 5-, 10- and 15- LBL deposition layers of TiO_2, respectively. The relative abundance and thickness of TiO_2 layers undergo an evident increase upon increasing the LBL deposited TiO_2 layers on the CuO NNA films. Upon 5-LBL repetition deposition of TiO_2, small papillary hills are spotted over the CuO NNA-coated copper meshes (Figs. 3a1 and 3a2), and abundant TiO_2 nanopartilces are clearly observed to be distributed over the CuO nanoneedles (Fig. 3a3). Further increasing LBL-deposited TiO_2 to 10 layers, denser and more massive TiO_2 nanoparticles with a diameter range of 30 - 70 nm are present on the TiO_2*10 LBL/CuO NNA dual-coated copper meshes (Figs. 3b1 and 3b2), thus leading to the increase in the average diameters of CuO nanoneedle (Fig. 3b3). The protruding TiO_2 nanoparticles are bestrewed over the surfaces of CuO nanoneedles (Fig. 3b3). The lumpy aggregates of TiO_2 are densely and uniformly covered on the surfaces of TiO_2*15 LBL/CuO NNA dual-coated copper meshes (Figs. 3c1-c3), leading to a more hierarchical micro/nano-structures on the copper meshes. It has been found that the nanoscale thickness of TiO_2 monolayer by the proposed LBL self-assembly deposition process is circa 1.5-2.0 nm [37]. Previous studies have reported that the thickness of a ten-LBL layer is around 22 nm [35]. Taking into account of different surface conditions between mesh and flat substrates, the thickness of TiO_2 multilayer coatings formed on the TiO_2*15 LBL/CuO NNA dual-coated copper meshes are supposed to be in a range from 20 to 30 nm. The vertically-grown CuO preserves their nanoneedle-like morphology even after 15-LBL deposition of TiO_2 (Fig. 3c2), although dense and thick TiO_2 multilayer coatings are accumulated

over the CuO nanoneedles. Taken together, the nanostructured TiO_2/CuO NNA dual coatings have been successfully fabricated by LBL deposition and subsequent cailcination process, and the deposition amount of TiO_2 is possibly positively correlated with the LBL-deposited TiO_2 layers. The hierarchical structures of the as-fabricated dual coatings along with microscale mesh wires are essential for the extreme wetting behaviors.

To quantitatively ascertain the dependence of deposition amount of TiO_2 on the repetition number of LBL deposition process, EDS spectra of the TiO_2*5 LBL/CuO, TiO_2*10 LBL/CuO, and TiO_2*15 LBL/CuO NNA dual-coated copper meshes were recorded, and the SEM images and the corresponding EDS spectra are shown in Fig. S2 (ESI), respectively. In comparison with EDS spectrum of the $Cu(OH)_2$ NNA--coated copper mesh (Fig. S2a), the appearance of additional signals of Ti element on the EDS spectra of the TiO_2/CuO NNA dual-coated copper meshes demonstrates the successful deposition of TiO_2 multilayer (Figs. S2b-2d). The respective atomic percentage of Ti element is circa 1.63%, 2.52% and 3.40% for the TiO_2*5 LBL/CuO, TiO_2*10 LBL/CuO, and TiO_2*15 LBL/CuO NNA dual-coated copper meshes, indicating that the deposition amount of TiO_2 undergoes a substantial increase with increasing the LBL deposition times. The LBL-deposited TiO_2 layers endow the as-fabricated copper meshes with the photo-catalytic functionality to achieve self-cleaning ability, by which the oily contaminant can be photodegradated to recover superwetting surfaces of the as-fabricated copper for recycle use.

3.2.2 XRD pattern.

The most common forms of the prototypical photocatalyst TiO_2 are anatase- and rutile-crystal structures. Based on the fact that the anatase TiO_2 is a better photocatalyst than the rutile TiO_2, and the phase transformation from anatase to rutile

is at a temperature range of 600-700^{o}C [38, 39], amorphous TiO_2/$Cu(OH)_2$ NNA dual coatings were transformed into crystalline phase by calcinations at 550^{o}C in this study. Fig. 4 shows the respective XRD pattern of the CuO NNA-coated mesh and TiO_2/CuO NNA dual-coated copper meshes with different TiO_2-deposited layers. The CuO NNA-coated copper meshes are obtained by the annealing dehydration treatment of $Cu(OH)_2$ NNA at 150^{o}C using a similar procedure described in our previous study.[30] As shown in Fig. 4a, the weak diffraction peaks marked by hearts with 2θ at 35.5^{o} (002) and 38.7^{o} (111) are attributed to the monoclinic phase of CuO (JCPDS card no. 05-0661), whilst three strong diffraction peaks marked by solid circles with 2θ at 43.4^{o} (111), 50.6^{o} (200) and 74.3^{o} (220) are associated with the pure copper substrates. This results suggests that only small amount of CuO NNA obtained by low-temperature annealing treatment is in polycrystalline form. For the TiO_2/CuO NNA dual-coated copper meshes, six distinctive peaks of TiO_2 layers marked by rhombuses with 2θ at 25.3^{o}, 36.9^{o}, 48.2^{o}, 53.9^{o}, 62.1^{o} and 68.8^{o}, corresponding to anatase reflection planes [(101), (103), (200), (105), (213), and (116)], are found as per JCPDS 21-127, indicative of successful deposition of crystalline anatase TiO_2 (Figs. 4b-4d). Meanwhile, the relative intensity of the above six anatase facets undergoes a gradual increase with increasing the deposited TiO_2 layers, indicating that more anatase TiO_2 are formed on the TiO_2*15 LBL/CuO NNA dual-coated meshes. This result is well consistent with the above SEM observation that the deposition amount of anatase TiO_2 increase with the LBL deposition times. On the other hand, the dramatic increase in the relative intensity of CuO (002) and (111) crystal plane reveals complete crystallization of CuO NNA upon high-temperature calcination (Figs. 4b-4d). In addition, two more diffraction peaks with 2θ at 43.6^{o} (200) and 66.7^{o} (113) also supports that only CuO is present on the as-fabricated copper meshes. Thus, the as-fabricated copper meshes are ascertained to be loaded with crystalline anatase TiO_2

and CuO NNA dual coatings for desirable superwetting properties and photo-catalytic functionality.

3.2.3 XPS spectra.

The surface compositions were also determined by XPS characterization to ascertain the successful fabrication of nanostructured TiO_2/CuO NNA dual-coated Cu meshes. Fig. 5 shows the respective wide scan, O 1s, Cu 2p and Ti 2p core-level spectra of the TiO_2*15 LBL/CuO NNA-coated Cu meshes. The corresponding XPS spectra of the $Cu(OH)_2$ NNA-coated copper meshes are shown in Fig. S3 (ESI). The successful growth of $Cu(OH)_2$ NNA on the copper mesh can be deduced from the appearance of $Cu(OH)_2$ species (BE at 935.1 eV) on the curve-fitted Cu 2p core-level spectrum (Figs. S3c) and the predominant hydroxide species (BE at 531.6 eV) on the curve-fitted O 1s core-level spectrum (Figs. S3b). In comparison with wide scan of the $Cu(OH)_2$ NNA-coated copper meshes (Fig. S3a), the appearance of additional signals with binding energy (BE) at 459 eV, attributable to the Ti 2p species, on the wide scan XPS spectrum of the TiO_2*15 LBL/CuO NNA-coated Cu meshes, indicative of the successful deposition of TiO_2 layers (Fig. 5a). The Cu 2p core-level spectrum of the TiO_2*15 LBL/CuO NNA-coated Cu meshes can be curve-fitted into two peak components with BEs at 932.6 and 933.8 eV (Fig. 5c), attributable to Cu and CuO species, respectively, indicative of the successful phase transformation of $Cu(OH)_2$ to CuO species upon the calcination treatment. This point is further confirmed by the presence of predominant oxide species (BE at 529.8 eV) on the curve-fitted O 1s core-level spectrum (Fig. 5b). The curve-fitted Ti 2p core-level spectrum consists of a spin-orbit-split doublet with BEs at 458.8 and 464.3 eV, attributable to the Ti $2p_{3/2}$ and Ti $2p_{1/2}$ species, respectively. Thus, the successful fabrication of the nanostrucured TiO_2/CuO NNA dual-coated copper meshes has been confirmed.

3.3 Wettability characterization of TiO_2/CuO NNA dual-coated copper meshes.

The wetting behaviors of water and oils on the as-fabricated copper meshes were evaluated by the contact angle measurement. In air, the water wetting behaviors on the $Cu(OH)_2$ NNA-coated and TiO_2*15 LBL/CuO NNA-coated copper meshes are substantially enhanced as compared to the pretreated copper mesh, which has a water contact angle of 116^{o}C (ESI, Fig. S5a). Fig. 6 shows the time-resolved optical snapshots of dynamic contact process of a water droplet on the TiO_2*15 LBL/CuO NNA-coated copper meshes in air, whilst the corresponding optical snapshots of a water droplet on the $Cu(OH)_2$ NNA-coated copper meshes are displayed in Fig. S4 (ESI). As shown in Fig. S4, the water droplet with a water contact angle of 20.2^o, spreads rapidly and penetrates the copper mesh (within 33 ms), once it contacts with the surfaces of the $Cu(OH)_2$ NNA-coated copper meshes. The water droplet completely penetrates through the $Cu(OH)_2$ NNA-coated mesh within 66 ms (ESI, Fig. S4), indicating the good hydrophilicity and permeability of the $Cu(OH)_2$ NNA-coated meshes towards water. On the other hand, when the water droplet contacts the surfaces of the TiO_2*15 LBL/CuO NNA dual-coated copper meshes, it also exhibits a quick spread from a initial water contact angles of circa 45.7^o to 0^c within 99 ms (Fig. 6), and the water droplet completely penetrates copper mesh within circa 160 ms. However, the spreading and penetration of water droplets on the surfaces TiO_2/CuO NNA dual-coated copper meshes appear to be slightly slower than those on the $Cu(OH)_2$ NNA-coated mesh. This result is ascribed to higher surface density of hydroxyl groups (-OH) on the $Cu(OH)_2$ NNA-coated mesh than those on the TiO_2*15 LBL/CuO NNA-coated mesh. Taken together, the TiO_2/CuO dual-coated meshes have been confirmed to exhibit desirable superhydrophilicity and good water penetration ability, which is caused by the combined effect of the hydrophilic nature of the TiO_2/CuO dual coatings and the surface hierarchical nanostructures generated in the

electrochemical anodization and LBL assemble process. Meanwhile, the current combined process of anodization and LBL self-assembly enables these TiO_2/CuO NNA dual coatings to be readily deposited on the copper meshes with controllable thickness, microstructures and morphology.

The underwater oil wettability of the TiO_2*15 LBL/CuO NNA dual-coated copper meshes was determined by immersing the as-fabricated meshes in aqueous solution. Fig. 7 shows the oil contact angle and the corresponding droplet shapes of different types of oil, on the as-fabricated copper meshes. Obviously, the TiO_2*15 LBL/CuO NNA dual-coated copper mesh exhibits good underwater superoleophobic property towards oil, because all of the oil contact angles are larger than 150^o, such as dichloromethane of 162^o, n-hexane of 151^o, isooctane of 159^o, olive oil of 157^o, crude oil of 154^o and kerosene of 152^o, on the as-fabricated copper mesh. However, the pristine pretreated copper mesh exhibits oleophilic property with an oil contact angle of 18^o towards kerosene (ESI, Fig. S5b). It is worthwhile to point out that these oil droplets are fairly mobile over the surfaces of TiO_2*15 LBL/CuO NNA dual-coated copper meshes, and they are readily detached from the surface by gentle disturbance, indicative of low adhesion force between oil droplets and the mesh surfaces in the aqueous solution. Taking into account of the hierarchical nanostructure and superhydrophilic features of the TiO_2/CuO NNA dual-coated copper meshes, water can be easily trapped into the rough nanostructures when the as-fabricated TiO_2/CuO dual-coated mesh is immersed in aqueous solution, thus resulting in the formation of an oil/water/solid dual coating interface. These trapped water molecules will greatly decrease the contact area between the oil droplets and sold surface. This phenomenon can be interpreted by Cassie-Baxter equation as follows [20]:

$$cos\theta_{ow}^{'} = f \cdot cos\theta_{ow} + f - 1 \quad (7)$$

where $\theta_{ow}^{'}$ and θ_{ow} are the contact angles of an oil droplet on the TiO_2/CuO dual-coated and the pristine pretreated copper substrates, respectively, f is the area fraction of solid in contact with oil. In this study, kerosene is chosen as example oil to calculate the value of parameter f on the basis of $\theta_{ow}^{'} = 152^{o}$ and$\theta_{ow} = 114^{o}$, thus the f value is obtained to be circa 0.167, indicating that approximately 84% of contact area is the oil/water contact interface. Consequently, the high oil contact angles on the surfaces of the TiO_2*15 LBL/CuO NNA dual-coated copper mesh is ascribed to the formation of a water cushion between the oil droplets and micro-/nano-structured solid surface filled with water molecules in the interspaces, which offers a strong repulsive force between polar mesh surface (water and TiO_2/CuO coatings) and non-polar oil phase [19, 23]. On the other hand, the triple-phase contact line (TCL) is discontinuous in this composite contact model, hence, the oil adhesion of the surface is extremely low and the oil droplets are able to readily roll off the surface.

3.4 Determination of oil/water separation performance

The nanostructured TiO_2/CuO NNA dual-coated copper meshes have been demonstrated desirable underwater superoleophobicity and superhydrophilicity. A series of proof-of-concept studies were carried out to assess the separation capability of oil and water mixture. Fig. 8 shows the photographs of a separation process of kerosene-water mixture. The as-fabricated TiO_2/CuO coated copper mesh is fixed at the middle of the customized funnel-shaped device (Fig. 8a), and the mixture of kerosene (stained with oil red) and water (v:v, 1:1) is poured into the upper glass tube after the pre-wetting of the mesh with deionized water. The whole separation process is virtually completed instantly (refer to the Supplementary Movie S1). Meanwhile, this separation process is only driven by gravity, and no other external force is involved. Owing to the underwater superhydrophobicity of the as-fabricated mesh and

the higher density of water than kerosene, the water in the oil/water mixture penetrates rapidly through the copper mesh into the beneath beaker, while the kerosene is repelled by the superoleophobic mesh to retain above the copper mesh (Fig. 8a), thus resulting in the complete separation of water-kerosene mixture. It is clear that no visible oil is observed in the permeated water (Fig. 8b). The separation of water-kerosene mixture by using a large piece of as-fabricated copper mesh is illustrated in Fig. S6 (ESI), which further confirms the high separation efficiency of the TiO_2/CuO dual-coated copper mesh.

To further quantitatively determine separation efficiency and deep understanding the major influencing factors on the separation efficiency of oil/water mixtures, the effect of different TiO_2 layers and oil types on the separation performance of the TiO_2/CuO NNA dual-coated copper mesh is investigated by the measurement of water flux and oil residue content in the permeated water. The water flux is a key index to evaluate the permeability of mesh substrates, whilst the oil residue content is obtained by the measurement of COD value on a spectrometer oil content analyzer to evaluate the separation efficiency. In this study, the water flux *F* is determined under a fixed column of water, of which the volume of water (V) that penetrates through the copper mesh is fixed at 1 L, the exposed area (S) of copper mesh is fixed at 28.5 cm^2, and the flowing time (t) is recorded by a chronograph from the beginning of pouring oil/water mixture into the device to the moment of water completely dripped into the beaker. Thus, water flux *F* of the as-fabricated copper mesh is calculated using the above Equation 1.

Fig. 9 shows the change in water flux and oil residue content in the permeated water after the oil/water separation as a function of LBL-deposited TiO_2 layers and oil types of oil/water mixtures for the as-fabricated TiO_2/CuO NNA dual-coated copper

meshes. As shown in Fig. 9a, the water flux and oil residue content in the permeated water for the $Cu(OH)_2$ NNA-coated meshes are at circa 112 $kL \cdot m^{-2} \cdot h^{-1}$ and 63 ppm, respectively. With increase in the LBL-deposited TiO_2 layers, the water flux of kerosene/water mixture gradually decrease from around 100 $kL \cdot m^{-2} \cdot h^{-1}$ for the TiO_2*5 LBL/CuO dual-coated mesh to 85 $kL \cdot m^{-2} \cdot h^{-1}$ for the TiO_2*15 LBL/CuO dual-coated mesh (Fig. 9a). This result is well consistent with the above SEM data that the LBL deposition of TiO_2 layers causes the increase in the thickness of coating layers, which results in the decrease in mesh pore size of copper mesh. The more TiO_2 layers are deposited on the mesh substrates, the smaller the mesh pore size is. Despite that, the water flux of the mesh remains as high as circa 85 $kL \cdot m^{-2} \cdot h^{-1}$ even after 15 LBL-deposition of TiO_2 layers (Fig. 9a), indicating that the LBL-deposited TiO_2 multilayer have no significant effect on the water flux of copper meshes. Meanwhile, the oil residue content in the filtrate water undergoes an evident decrease from circa 40 ppm to 15 ppm upon increasing the LBL-deposited TiO_2 layers from 5 to 15 layers, indicative of the increase in the separation efficiency with LBL-deposited TiO_2 layers (Fig. 9a). This result is probably ascribed to the increase in hierarchical roughness, and thus the increase in underwater superoleophobicity of the copper mesh. Taken together, except for rendering the self-cleaning ability, the LBL-deposited TiO_2 layers also facilitate the formation of rougher hierarchical structures for the enhanced underwater superoleophobicity, whilst the permeability of the copper meshes is not substantially compromised. Therefore, the TiO_2*15 LBL/CuO NNA dual-coated copper mesh is chosen for the subsequent oil/water separation test.

A variety of oil/water mixtures, including hexane, isooctane, kerosene and olive oil, are used for separation test to determine the effect of oil types on the separation efficiency. As shown in Fig. 9b, the oil types have little effect on the water flux, as all the water fluxes of oil/water mixture flow remain higher than 85 $kL \cdot m^{-2} \cdot h^{-1}$ for these

oil/water mixtures. The highest water flux of circa 115 $kL \cdot m^{-2} \cdot h^{-1}$ is achieved for the isooctane/water mixture. On the other hand, the oil residue content of different oil/water mixtures is much different from each other, since the oil residue content of hexane or isooctane/water mixtures is as low as less than 10 ppm, whilst that of the olive oil/water mixture is higher than 60 ppm. This result is probably associated with different polarity of these oils. Hexane and isooctane are good nonpolar organic solvents with the polarity close to 0 [34,[26] while olive oil contains copious amount of unsaturated aliphatic acids with high polarity, some of which might be soluble in water.[15, 40] Hence, the complex ingredients of olive oil result in the increase in oil residue content in the permeated water for the olive oil/water mixture separation. The oil residue content of kerosene/water mixture is less than 20 ppm (Fig. 9b). Overall, these above oil/water mixtures have been efficiently separated by the TiO_2*15 LBL/CuO NNA dual-coated copper meshes, indicating that the as-fabricated copper mesh has a wide range of applications.

3.5 Self-cleaning property of the nanostructured TiO_2/CuO NNA dual-coated copper mesh.

Self-cleaning property is highly desirable for a separation mesh in order to realize recycling use and enhance its separation efficiency to oil-contaminated water. It has been widely accepted that anatase TiO_2 materials are regarded as one of the most promising photocatalysts to degrade organic contaminants [41]. Under ultraviolet (UV) light illumination, photo-electrons and holes are generated on the TiO_2 material surface, which subsequently react with water and oxygen to give rise to highly reactive superoxide anions and hydroxyl radicals [42]. These highly reactive species are capable of decomposing organic contaminants and fouling species that are adsorbed on the surface of separation meshes [43, 44]. To evaluate self-cleaning ability of the as-fabricated copper mesh, the kerosene-contaminated TiO_2*15

LBL/CuO NNA dual-coated copper meshes, which was obtained by continuous separation of kerosene/water mixture until dramatic increase in the oil residue content (COD value) and subsequently washed with copious amount of deionized water for 5 min, was subject to UV light illumination for a predetermined time (wavelength centered at 360 nm). The change in water contact angle in air with exposure time was recorded to determine the optimal UV illumination time, and the result is shown in Fig. S7 (ESI). It is evident that surface hydrophilicity of the mesh gradually recovers with exposure time, and the water contact angle returns to the original value of 0^o after 120 min of exposure. The superhydrophilicity recovery of the as-fabricated copper meshes in air is the result of photodecomposition removal of the surface-adsorbed kerosene. Under the visible light illumination, the as-prepared meshes also show photodegradation ability to kerosene contaminants, as water contact angles slowly decrease with increasing exposure time to around 10^o after 480 min. Taken together, the as-prepared mesh exhibit higher photo-catalytic activity under UV illumination than under visible light illumination. Thus, the optimal UV-illumination time of the regenerated copper mesh is proven to be 120 min.

To further ascertain the separation efficiency of regenerated copper mesh, the as-fabricated copper mesh was continuously utilized for three times to separate kerosene/water mixture at a volume of 5 L at each time prior to being regenerated under UV light illumination. Fig. 10a displays the change in oil residue content (COD value) in the permeated water after each oil/water separation process on the TiO_2*15 LBL/CuO NNA dual-coated copper meshes as a function of repeated usage time and UV-illuminated recycle time. Obviously, the first-run separation of kerosene/water mixture on the regenerated copper mesh shows a fairly high separation efficiency with the oil residue content less than 20 ppm for all the recycle uses, whilst the oil residue content of the second-run and third-run separation reaches as high as more than 175 ppm and 250 ppm, respectively, suggesting the occurrence of oil contamination (or

the adsorption of kerosene) on the mesh surface upon increasing usage times. The good self-cleaning property of the TiO_2*15 LBL/CuO NNA dual-coated copper meshes can be deduced from the dramatic decrease in oil residue content from more than 250 ppm in the third-run separation process to 20 ppm after UV light illumination (Fig. 10a). In fact, the oil contaminants gradually accumulate on the mesh surfaces with continuous processing oil/water separation, thus resulting in the gradual loss of separation capability.

On the other hand, the corresponding water contact angles in air of kerosene-contaminated TiO_2*15 LBL/CuO NNA dual-coated copper meshes upon before and after UV light illumination are measured to further verify the self-cleaning property. Fig. 10b shows the change in water contact angle on the TiO_2*15 LBL/CuO NNA dual-coated copper mesh upon seven cycles of kerosene contamination and UV illumination recovery. After the kerosene contamination, the surface wettablity of the copper mesh becomes hydrophobic with water contact angels in a range of 100 – 120^o. Upon UV illumination recovery, the TiO_2*15 LBL/CuO NNA dual-coated copper meshes still exhibit desirable superhydrophilicity with water contact angles close to 0^o and underwater superoleophobicity, indicating the good reproducibility and stability of the nanostructured TiO_2/CuO dual coatings under UV light illumination, whilst the $Cu(OH)_2$ NNA-coated mesh exhibit no self-cleaning property, as no change in the water contact angle can be observed after UV light illumination (ESI, Fig. S9a). On the other hand. the poor recovery of superhydrophlicity for the as-prepared meshes is observed on the TiO_2*15 LBL/CuO NNA dual-coated mesh under visible light illumination, and the water contact angles after visible light increase to more than 40^o after three cycles, as shown in Fig. 9Sb (ESI). Taken together, the self cleaning ability derived from LBL-deposited TiO_2 layer under UV light illumination has proven to guarantee the as-fabricated meshes with the same performance as before the

contamination, hence, this dual oxide layers-coated copper mesh might be used over again for the highly efficient separation of a wide range of oil/water mixtures.

The optical property of the as-fabricated copper meshes is further investigated to seek deep understanding of photo-catalytic activity of the nanostructured TiO_2/CuO dual coatings. The diffused reflectance UV-visible spectrum and the corresponding Tauc plot of the TiO_2*15 LBL/CuO NNA dual-coated copper mesh are shown in Fig. S11. A strong absorbance peak before 300 nm regions (centered at 275 nm) is ascribed to TiO_2 UV absorption regions, while a minor peak in the wavelength range of 400 - 500 nm indicates a noticing absorption of visible light (Fig. 11a), which is probably associated with the CuO layers.[33, 45] Upon analyzing the absorption coefficients of the TiO_2/CuO dual coatings by Tauc approach, which is the most widespread method to determine the optical properties of semiconductors, the direct band gap of the semiconductors are calculated by using the following equation [46]:

$$\alpha = \frac{C(\square v - E_g^{bulk})^{1/2}}{\square v} \quad (8)$$

where α is the absorption coefficient, C is a constant, *hv* is the photon energy, and E_g^{bulk} is the band gap. As shown in Fig. 11b, extrapolation of the linear region gives rise to two absorption bands at 2.89 and 2.61 eV (Fig. 11b), attributable to the direct transition within the TiO_2 and CuO thin layers, respectively. In comparison with the band gap at 3.2 eV for pure TiO_2, the red shift of band gap for the TiO_2 layers indicates that incorporation of CuO layers might act as dopant in the as-fabricated TiO_2/CuO nano-photocatalyst. This result is consistent with the Tauc-estimated band gap of CuO NNA-coated copper mesh at circa 2.5 eV, as shown in Fig. S10 (ESI). Overall, the above results provide a strong evidence of absorption of UV and visible light with photo-catalytic property of the nanostructured TiO_2/CuO NNA dual-coated copper mesh.

3.6 Stability and durability of the nanostructured TiO_2/CuO NNA dual-coated

copper mesh.

For practical applications in oily wastewater, it is appropriate to emphasize on the stability and durability of the as-fabricated superwetting meshes. The fact that the nanostructured TiO_2/CuO NNA dual coatings are entirely inorganic guarantees the integrity of the dual oxide coatings during the oil/water separation and UV-based self-cleaning treatment. Furthermore, in this study, the TiO_2/CuO dual-coated meshes are subject to deionized water for a predetermined exposure time to evaluate the durability of their superhydrophilicity and underwater superoleophobicity. Fig. 12 shows the respective change in water contact angle in air and underwater oil contact angle as a function of exposure time in deionized water for the TiO_2*15 LBL/CuO NNA dual-coated copper meshes. It is easily observed that the superhydrophilicity and underwater superoleophobicity of the as-fabricated copper meshes remain unchanged throughout 7 days of exposure time, since the water contact angles in air are always close to 0^o throughout, whilst the underwater oil contact angle are always more than 150^o. Thus, the good stability and durability of the nanostructured TiO_2/CuO dual-coated copper meshes are confirmed.

Conclusions

A novel nanostructured TiO_2/CuO dual-coated copper mesh with superhydrophilic, underwater superoleophobic, and self-cleaning properties was fabricated by a combined process of electrochemical anodization and layer-by-layer self-assembly deposition. Success in each fabrication step was ascertained by characterization of SEM-EDX, XRD, XPS, water contact angles and underwater oil contact angles. The as-fabricated copper meshes demonstrated high separation efficiency to oil/water mixtures with oil residue contents less than 20 ppm, high permeability with water flux of more than 80 $kL \cdot h^{-1} \cdot m^{-2}$, as well as desirable self-cleaning ability to be conveniently regenerated under UV illumination for recycle usage. With the inherent advantages of good stability and high mechanical strength of superwettting inorganic coatings and versatility to various oil/water mixtures, the current nanostructured TiO_2/CuO dual-coated copper mesh offers a novel and promising separation material for the remediation of oily wastewater.

Acknowledgements

The authors would like to acknowledge The National Key Research and Development Program of China (2016YFB0301701) and the financial assistance of National Natural Science Foundation of China (NO. 21676169).

References & Notes

[1] Y.L. Shi, W. Yang, X.J. Feng, Y.S. Wang, G.R. Yue, S.P. Jin, Fabrication of superhydrophobic-superoleophilic copper mesh via thermal oxidation and its application in oil–water separation, Appl. Surf. Sci. 367 (2016) 493-499.
[2] J. Song, Y. Lu, J. Luo, S. Huang, L. Wang, W. Xu, I.P. Parkin, Barrel-shaped oil skimmer designed for collection of oil from spills, Adv. Mater. Interf. 2 (2015) 1500350.
[3] J. Saththasivam, K. Loganathan, S. Sarp, An overview of oil–water separation using gas flotation systems, Chemosphere 144 (2016) 671-680.
[4] C.T. Liu, Y.L. Liu, pH-Induced switches of the oil- and water-selectivity of crosslinked polymeric membranes for gravity-driven oil-water separation, J. Mater. Chem. A 4 (2016) 13543-13548.
[5] C. Su, H. Yang, S. Song, B. Lu, R. Chen, A magnetic superhydrophilic/oleophobic sponge for continuous oil-water separation, Chem. Eng. J. 309 (2017) 366-373.
[6] P. Cañizares, F. Martínez, C. Jiménez, C. Sáez, M.A. Rodrigo, Coagulation and electrocoagulation of oil-in-water emulsions, J. Hazard. Mater.151 (2008) 44-51.
[7] J.S. Eow, M. Ghadiri, A.O. Sharif, T.J. Williams, Electrostatic enhancement of coalescence of water droplets in oil: a review of the current understanding, Chem. Eng. J. 84 (2001) 173-192.
[8] Y. Zhu, F. Zhang, D. Wang, X.F. Pei, W. Zhang, J. Jin, A novel zwitterionic polyelectrolyte grafted PVDF membrane for thoroughly separating oil from water with ultrahigh efficiency, J. Mater. Chem. A 1 (2013) 5758.
[9] E.C. Cho, C.W. C. Jian, H.C. Chen, KS. Chuang, J.H. Zheng, Y.S. Hsiao, K.C. Lee, J.H. Huang, Robust multifunctional superhydrophobic coatings with enhanced water/oil separation, self-cleaning, anti-corrosion, and anti-biological adhesion, Chem. Eng. J. 314 (2017) 347-357.
[10] D. Zang, F. Liu, M. Zhang, X. Niu, Z. Gao, C. Wang, Superhydrophobic coating on fiberglass cloth for selective removal of oil from water, Chem. Eng. J. 262 (2015) 210-216.
[11] A. Raza, B. Ding, G. Zainab, M. El-Newehy, S.S. Al-Deyab, J. Yu, In situ cross-linked superwetting nanofibrous membranes for ultrafast oil–water separation, J. Mater. Chem. A 2 (2014) 10137.
[12] J.J. Li, L.T. Zhu, Z.H. Luo, Electrospun fibrous membrane with enhanced swithchable oil/water wettability for oily water separation, Chem. Eng. J. 287 (2016) 474-481.
[13] S. Rezaei, I. Manoucheri, R. Moradian, B. Pourabbas, One-step chemical vapor deposition and modification of silica nanoparticles at the lowest possible temperature and superhydrophobic surface fabrication, Chem. Eng. J. 252 (2014) 11-16.
[14] M. Liu, J. Li, Z. Guo, Polyaniline coated membranes for effective separation of oil-in-water emulsions, J. Colloid Interf. Sci. 467 (2016) 261-270.
[15] Z. Cheng, H. Lai, Y. Du, K. Fu, R. Hou, C. Li, N. Zhang, K. Sun, pH-induced reversible wetting transition between the underwater superoleophilicity and superoleophobicity, ACS Appl. Mater. Interf 6 (2014) 636-641.
[16] Z. Cheng, H. Liu, H. Lai, Y. Du, K. Fu, C. Li, J. Yu, N. Zhang, K. Sun, regulating underwater oil adhesion on superoleophobic copper films through assembling

n-alkanoic acids, ACS Appl. Mater. Interf 7 (2015) 20410-20417.
[17] J. Zeng, Z. Guo, Superhydrophilic and underwater superoleophobic MFI zeolite-coated film for oil/water separation, Colloid Surfaces A 444 (2014) 283-288.
[18] C. Zhou, J. Cheng, K. Hou, A. Zhao, P. Pi, X. Wen, S. Xu, Superhydrophilic and underwater superoleophobic titania nanowires surface for oil repellency and oil/water separation, Chem. Eng. J. 301 (2016) 249-256.
[19] Z. Xue, S. Wang, L. Lin, L. Chen, M. Liu, L. Feng, L. Jiang, A novel superhydrophilic and underwater superoleophobic hydrogel-coated mesh for oil/water separation, Adv. Mater. 23 (2011) 4270-4273.
[20] Q. Wen, J. Di, L. Jiang, J. Yu, R. Xu, Zeolite-coated mesh film for efficient oil–water separation, Chem. Sci. 4 (2013) 591-595.
[21] C.R. Crick, J.A. Gibbins, I.P. Parkin, Superhydrophobic polymer-coated copper-mesh; membranes for highly efficient oil-water separation, J. Mater. Chem. A 1 (2013) 5943-5948.
[22] Y. Lu, S. Sathasivam, J. Song, F. Chen, W. Xu, C.J. Carmalt, I.P. Parkin, Creating superhydrophobic mild steel surfaces for water proofing and oil-water separation, J. Mater. Chem. A 2 (2014) 11628-11634.
[23] H. Zhu, D. Chen, N. Li, Q. Xu, H. Li, J. He, J. Lu, Dual-layer copper mesh for integrated oil-Water separation and water purification, Appl. Cataly.B 200 (2017) 594-600.
[24] X. Du, X. Huang, X. Li, X. Meng, L. Yao, J. He, H. Huang, X. Zhang, Wettability behavior of special microscale ZnO nail-coated mesh films for oil-water separation, J. Colloid Interf. Sci. 458 (2015) 79-86.
[25] E. Zhang, Z. Cheng, T. Lv, Y. Qian, Y. Liu, Anti-corrosive hierarchical structured copper mesh film with superhydrophilicity and underwater low adhesive superoleophobicity for highly efficient oil-water separation, J. Mater. Chem. A 3 (2015) 13411-13417.
[26] F. Zhang, W.B. Zhang, Z. Shi, D. Wang, J. Jin, L. Jiang, Nanowire-haired inorganic membranes with superhydrophilicity and underwater ultralow adhesive superoleophobicity for high-efficiency oil/water separation, Adv Mater 25 (2013) 4192-4198.
[27] Z.Y. Luo, K.X. Chen, Y.-Q. Wang, J.-H. Wang, D.C. Mo, S.S. Lyu, Superhydrophilic nickel nanoparticles with core–shell structure to decorate copper mesh for efficient oil/water separation, J. Phys. Chem. C 120 (2016) 12685-12692.
[28] T. Darmanin, E.T. de Givenchy, S. Amigoni, F. Guittard, Superhydrophobic surfaces by electrochemical processes, Adv Mater 25 (2013) 1378-1394.
[29] T.A. Otitoju, A.L. Ahmad, B.S. Ooi, Superhydrophilic (superwetting) surfaces: A review on fabrication and application, J. Ind. Eng.Chem. 47 (2017) 19-40.
[30] F. Xiao, S. Yuan, B. Liang, G. Li, S.O. Pehkonen, T. Zhang, Superhydrophobic CuO nanoneedle-covered copper surfaces for anticorrosion, J. Mater. Chem. A 3 (2015) 4374-4388.
[31] Y. Lai, Y. Tang, J. Gong, D. Gong, L. Chi, C. Lin, Z. Chen, Transparent superhydrophobic/superhydrophilic TiO2-based coatings for self-cleaning and anti-fogging, J. Mater.Chem. 22 (2012) 7420.
[32] L. Zhang, Y. Zhong, D. Cha, P. Wang, A self-cleaning underwater superoleophobic mesh for oil-water separation, Sci. Rep. 3 (2013) 2326.
[33] H. Liu, A. Raza, A. Aili, J. Lu, A. AlGhaferi, T. Zhang, Sunlight-sensitive anti-fouling nanostructured TiO_2 coated Cu meshes for ultrafast oily water treatment, Sci Rep 6 (2016) 25414.

[34] X. Du, S. You, X. Wang, Q. Wang, J. Lu, Switchable and simultaneous oil/water separation induced by prewetting with a superamphiphilic self-cleaning mesh, Chem. Eng. J. 313 (2017) 398-403.
[35] S.J. Yuan, F.J. Xu, S.O. Pehkonen, Y.P. Ting, E.T. Kang, K.G. Neoh, Biocorrosion behavior of titanium oxide/butoxide-coated stainless steel, J. Electrochem. Soc 155 (2008) C196.
[36] S.J. Yuan, S.O. Pehkonen, Microbiologically influenced corrosion of 304 stainless steel by aerobic Pseudomonas NCIMB 2021 bacteria: AFM and XPS study, Colloid Surfaces B 59 (2007) 87-99
[37] M.C. Advincula, D. Petersen, F. Rahemtulla, R. Advincula, J.E. Lemons, Surface analysis and biocorrosion properties of nanostructured surface sol–gel coatings on Ti6Al4V titanium alloy implants, Journal of Biomedical Materials Research Part B: Applied Biomaterials 80B (2007) 107-120.
[38] T. Luttrell, S. Halpegamage, J. Tao, A. Kramer, E. Sutter, M. Batzill, Why is anatase a better photocatalyst than rutile?--Model studies on epitaxial TiO2 films, Sci. Rep. 4 (2014) 4043.
[39] D.A.H. Hanaor, C.C. Sorrell, Review of the anatase to rutile phase transformation, J. Mater.Sci. 46 (2010) 855-874.
[40] M.W. Lee, S. An, S.S. Latthe, C. Lee, S. Hong, S.S. Yoon, Electrospun polystyrene nanofiber membrane with superhydrophobicity and superoleophilicity for selective separation of water and low viscous oil, ACS Appl.Mater. Interf. 5 (2013) 10597-10604.
[41] A. Manivel, S. Naveenraj, P.S. Sathish Kumar, S. Anandan, CuO-TiO_2 nanocatalyst for photodegradation of acid red 88 in aqueous solution, Sci. Adv. Mater. 2 (2010) 51-57.
[42] A.L. Linsebigler, G. Lu, J.T. Yates, Photocatalysis on TiO2 surfaces: principles, mechanisms, and selected results, Chem. Rev. 95 (1995) 735-758.
[43] X. Chen, S.S. Mao, Titanium dioxide nanomaterials: synthesis, properties, modifications, and applications, Chemical reviews 107 (2007) 2891-2959.
[44] T.L. Thompson, J.T. Yates, Surface science studies of the photoactivation of TiO2 new photochemical processes, Chemical Reviews 106 (2006) 4428-4453.
[45] S.B. Wang, C.H. Hsiao, S.J. Chang, K.T. Lam, K.H. Wen, S.C. Hung, S.J. Young, B.R. Huang, A CuO nanowire infrared photodetector, Sensors and Actuators A: Physical 171 (2011) 207-211.
[46] M.E. Sánchez-Vergara, J.C. Alonso-Huitron, A. Rodriguez-Gómez, J.N. Reider-Burstin, Determination of the optical GAP in thin films of amorphous dilithium phthalocyanine using the Tauc and Cody models, Molecules 17 (2012) 10000-10013.

Figure Legends

Fig. 1 Schematic illustration of a three-step fabrication process for the TiO_2/CuO dual-coated copper meshes: (a) electrochemical anodization of the surfaces of copper meshes to produce $Cu(OH)_2$ nanoneedle arrays (NNA), (b) deposition of $Ti(OH)_4$ layers by sol-gel layer-by-layer self-assembly process on the $Cu(OH)_2$ NNA-coated copper meshes, and (c) calcination of $Ti(OH)_4$/$Cu(OH)_2$ dual coatings to obtain the nanostructured TiO_2/CuO dual-coated copper meshes.

Fig. 2 SEM images at different magnifications (300×, 1000× and 5000×) for the anodized $Cu(OH)_2$ NNA-coated copper meshes obtained in the (a1-a3) 1 mol L^{-1} KOH solution, (b1-b3) the mixture solution of 1 mol L^{-1} KOH and 0.5 mol L^{-1} NH_4Cl, and (c1-c3) the mixture solution of 1 mol L^{-1} KOH and 0.5 mol L^{-1} NH_4F at a current density of 2.0 mA cm^{-2} and 10^{o}C for 30 min.

Fig. 3 SEM images at different magnifications (300×, 10000× and 50000×) for the (a1-a3) TiO_2*5 LBL/CuO NNA dual-coated copper meshes, (b1-b3) TiO_2*10 LBL/CuO NNA dual-coated copper meshes and (c1-c3) TiO_2*15 LBL/CuO NNA dual-coated copper meshes.

Fig. 4 XRD patterns of the (a) CuO NNA-coated copper meshes obtained by annealing dehydration at 150^{o}C, (b) TiO_2*5 LBL/CuO NNA dual-coated copper meshes, (c) TiO_2*10 LBL/CuO NNA dual-coated copper meshes and (d) TiO_2*15 LBL/CuO NNA dual-coated copper meshes..

Fig. 5 (a) Wide scan, (b) O 1s, (c) Cu 2p and (d) Ti 2p core-level XPS spectra of the TiO_2*15 LBL/CuO NNA dual-coated copper meshes.

Fig. 6 Time-resolved snapshots from contact angle measurement video of a water droplet contacting on the TiO_2*15 LBL/CuO NNA dual-coated copper meshes in air. The photographs were captured using high-speed photography with 33 ms per frame.

Fig. 7 Contact angles of a series of typical oil droplets and the respective optical snapshot of oil droplets on the TiO_2*15 LBL/CuO NNA dual-coated copper meshes in aqueous media.

Fig. 8 (a) Photographs of oil-water mixture separation using the TiO_2*15 LBL/CuO NNA dual-coated copper meshes. The meshes were pre-wetted by deionized water flowing through the fixed copper meshes between two glass tubes. A mixture of kerosene and water was poured into the upper glass tube. The separation of oil-water mixture was achieved by water passing through the mesh, together with kerosene staying on top of the mesh. (b) optical photos of the mixture of kerosene and water, collected water and kerosene after separation operations. The complete separation of oil and water was ascertained by the fact that no visible oil and water was observed in the collected water and oil, respectively.

Fig. 9 The change in water flux and oil residue content (COD value) in the permeated water after the oil/water separation test as a function of (a) TiO_2 layers and (b) oil types of oil/water mixture for the as-fabricated TiO_2/CuO NNA dual-coated copper meshes.

Fig. 10 (a) The change in oil residue content (COD value) in the permeated water after the oil/water separation process using the TiO_2*15 LBL/CuO NNA dual-coated copper meshes as a function of repeated usage time and UV-illuminated recycle time. The mesh was used thrice for separating five litres of the oil and kerosene mixture solution at each time. The contaminated meshes were recovered by UV illumination with a 500 W mercury light, (b) the change in water contact angle on the TiO_2*15 LBL/CuO NNA dual-coated copper mesh upon seven cycles of kerosene contamination and UV illumination recovery.

Fig. 11 (a) UV-visible spectra and (b) Tauc plot for the band gap measurement of the TiO_2*15 LBL/CuO NNA -coated Cu meshes.

Fig. 12 The change in WCA and underwater OCA as a function of exposure time in deionized water, together with the respective optical snapshots of oil droplets and water droplets on the TiO_2*15 LBL/CuO NNA dual-coated copper meshes.

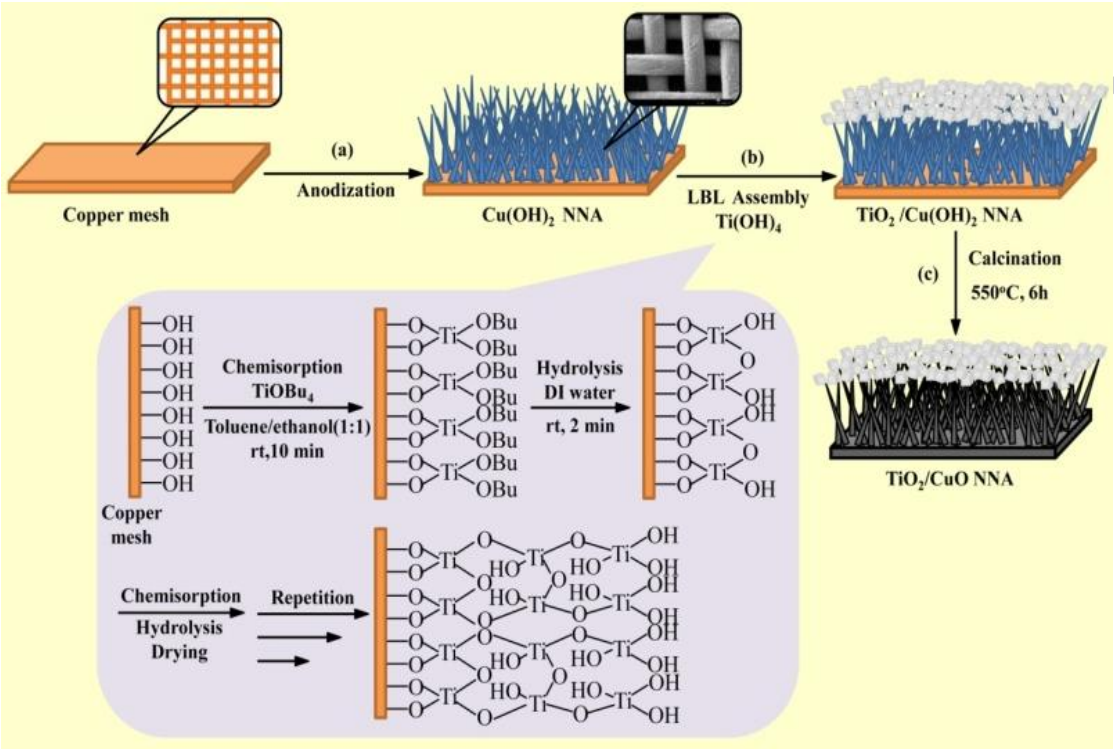

Figure 1

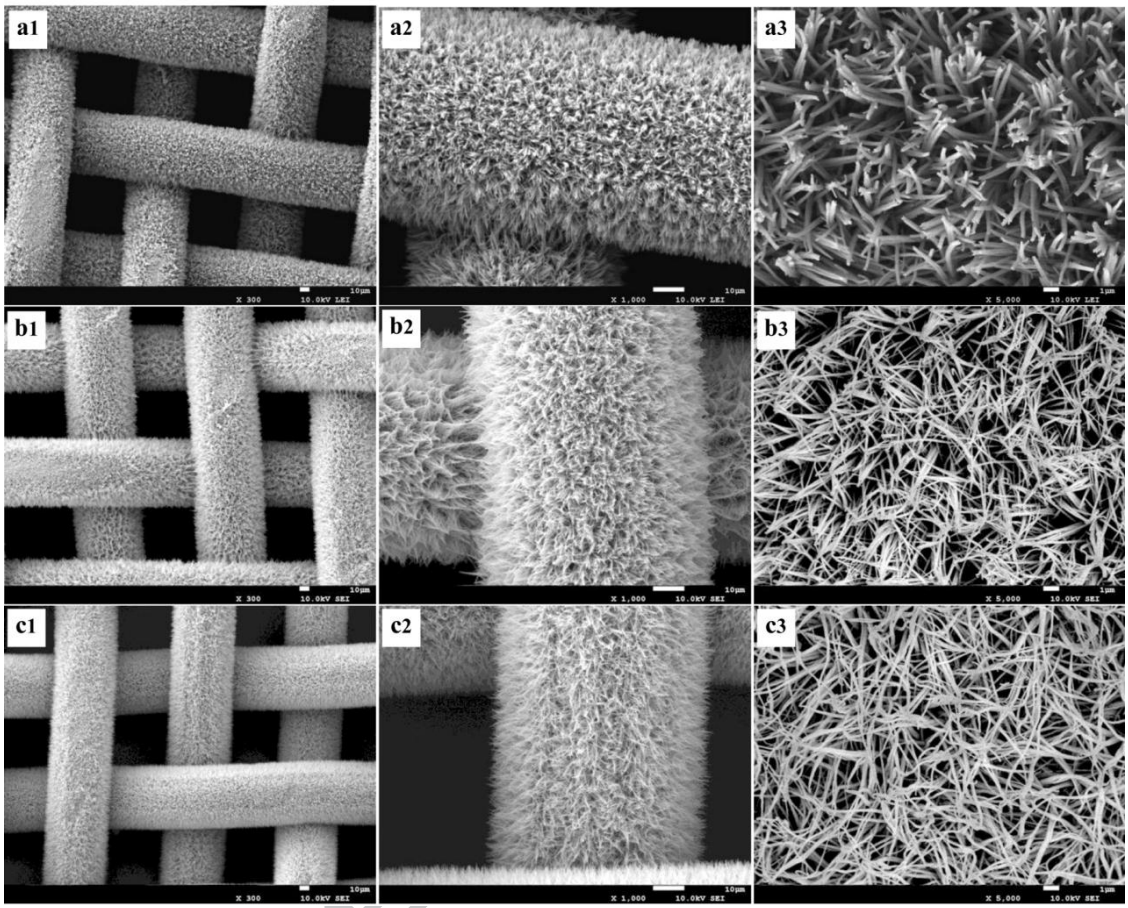

Figure 2

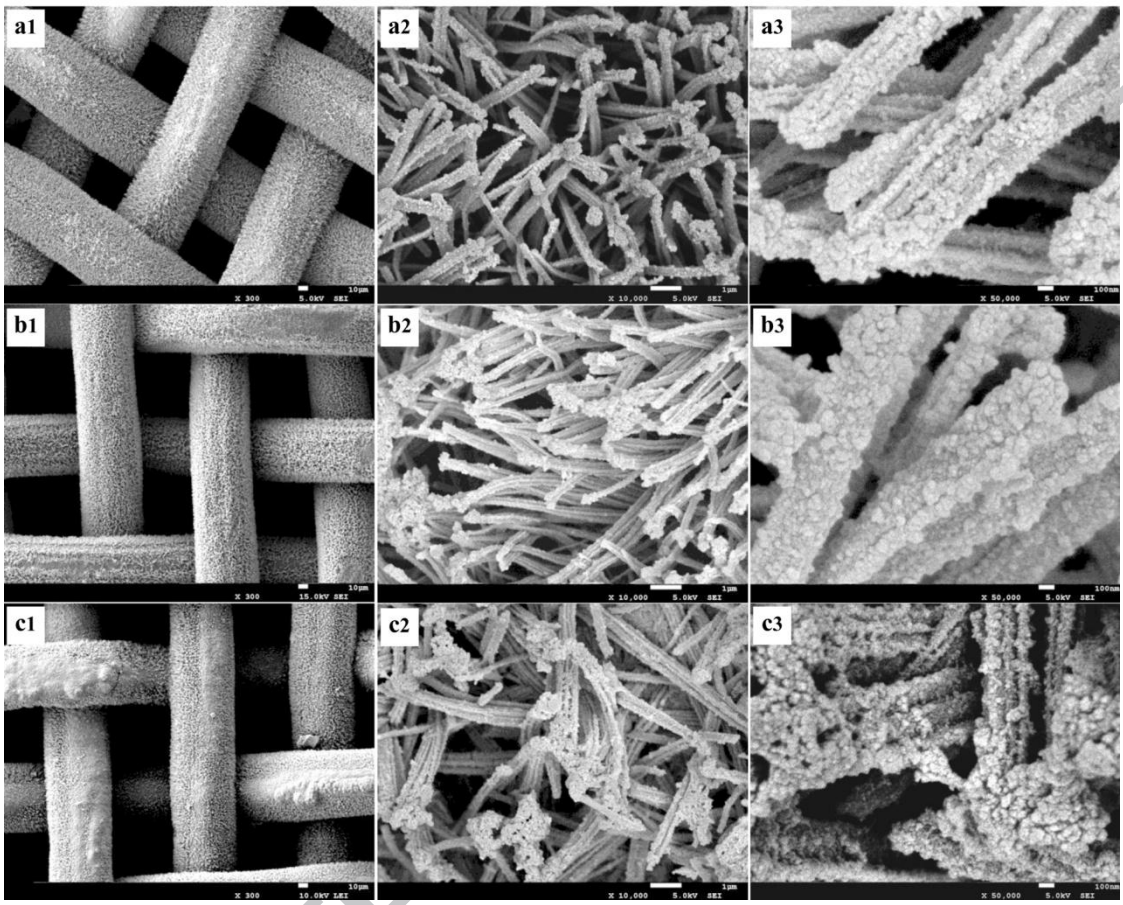

Figure 3

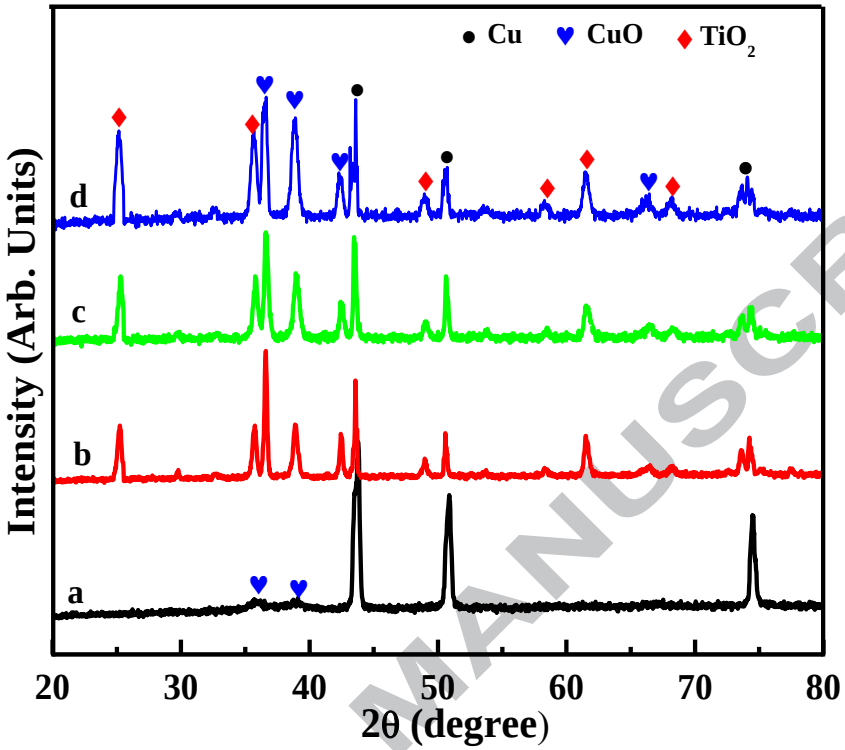

Figure 4

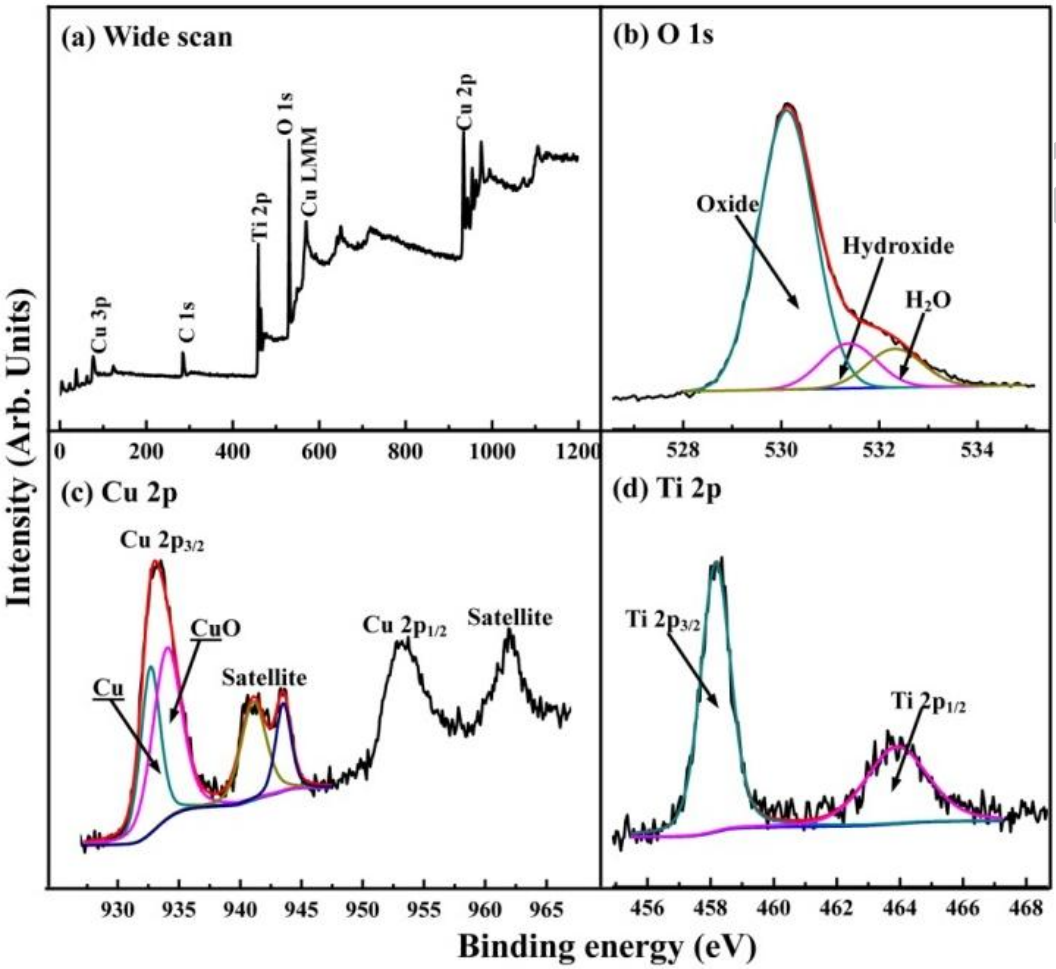

Figure 5

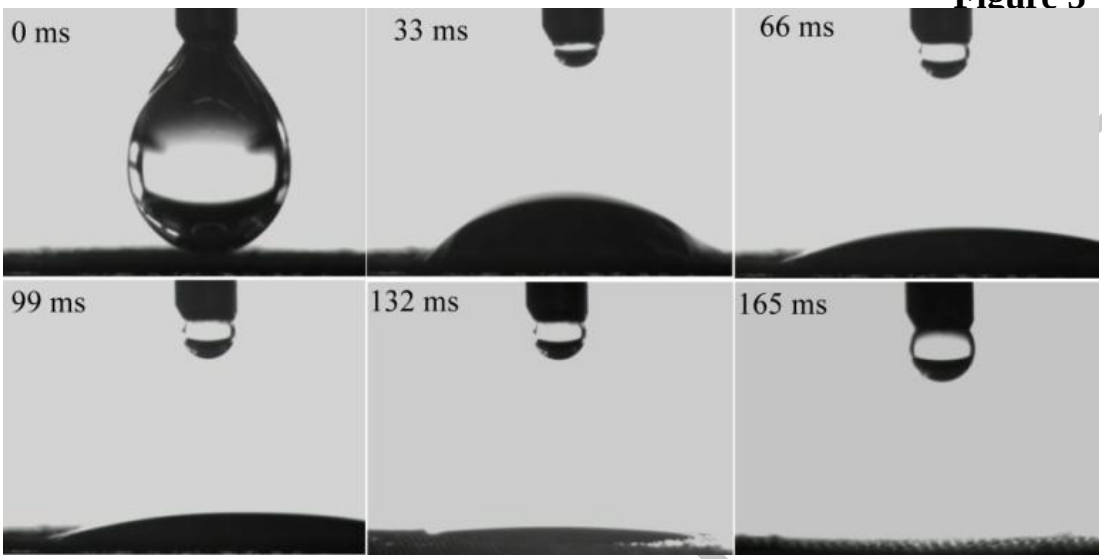

Figure 6

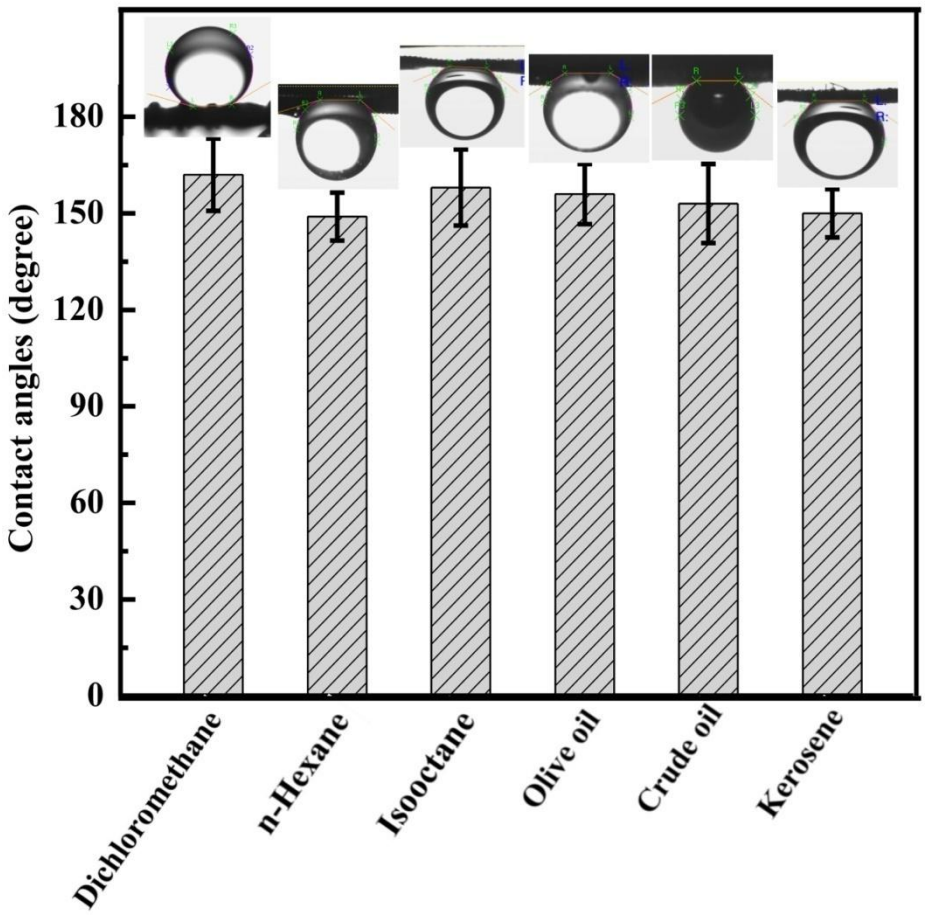

Figure 7

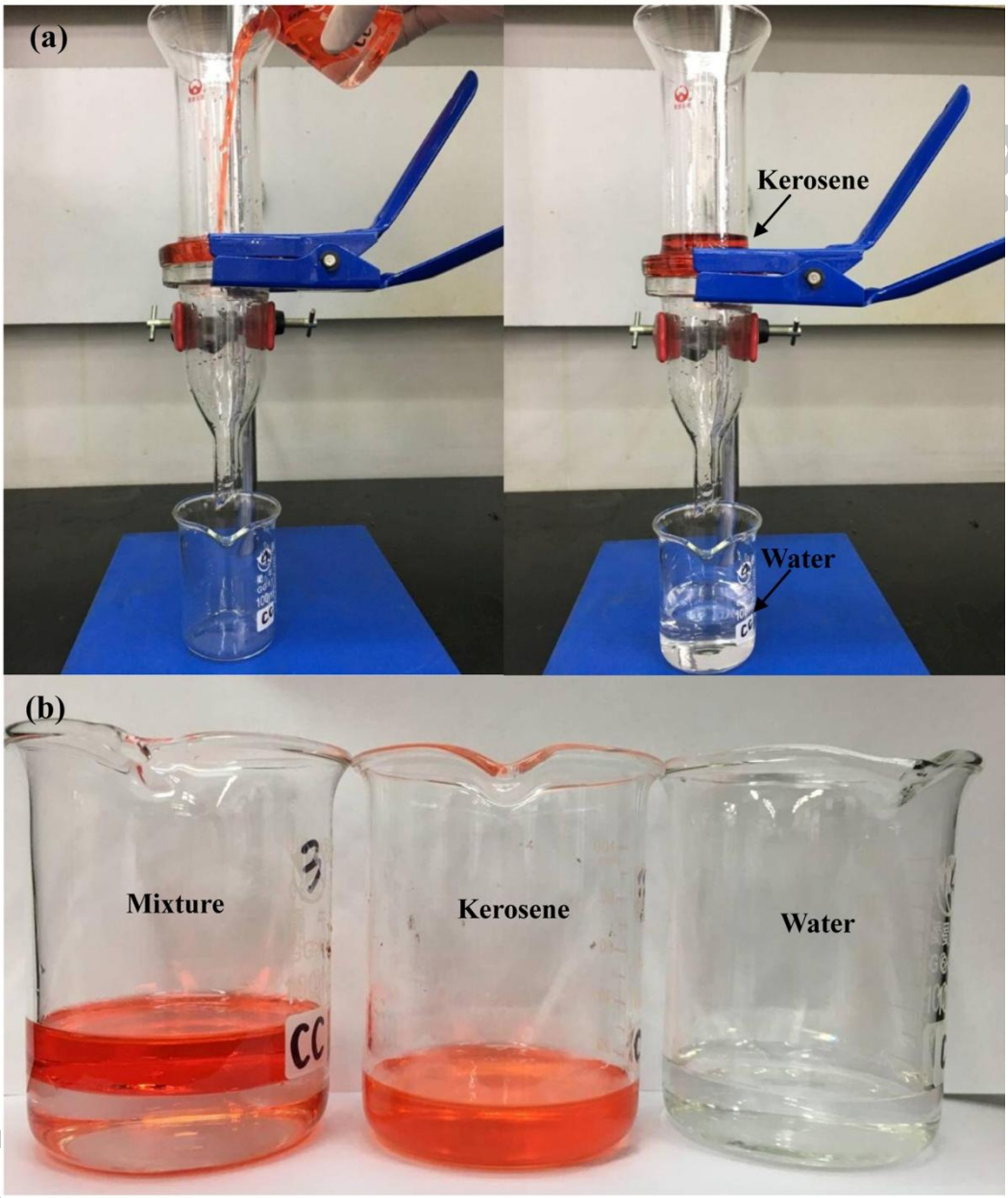

Figure 8

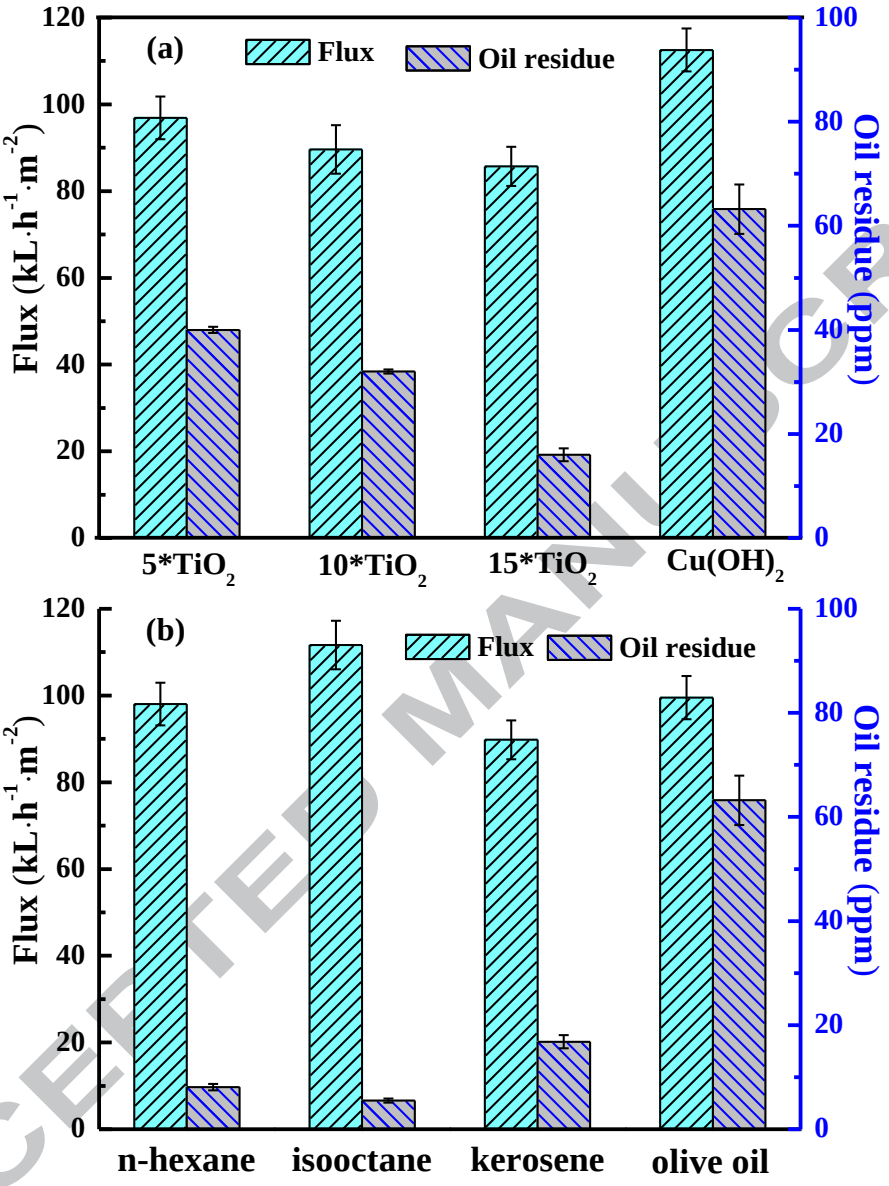

Figure 9

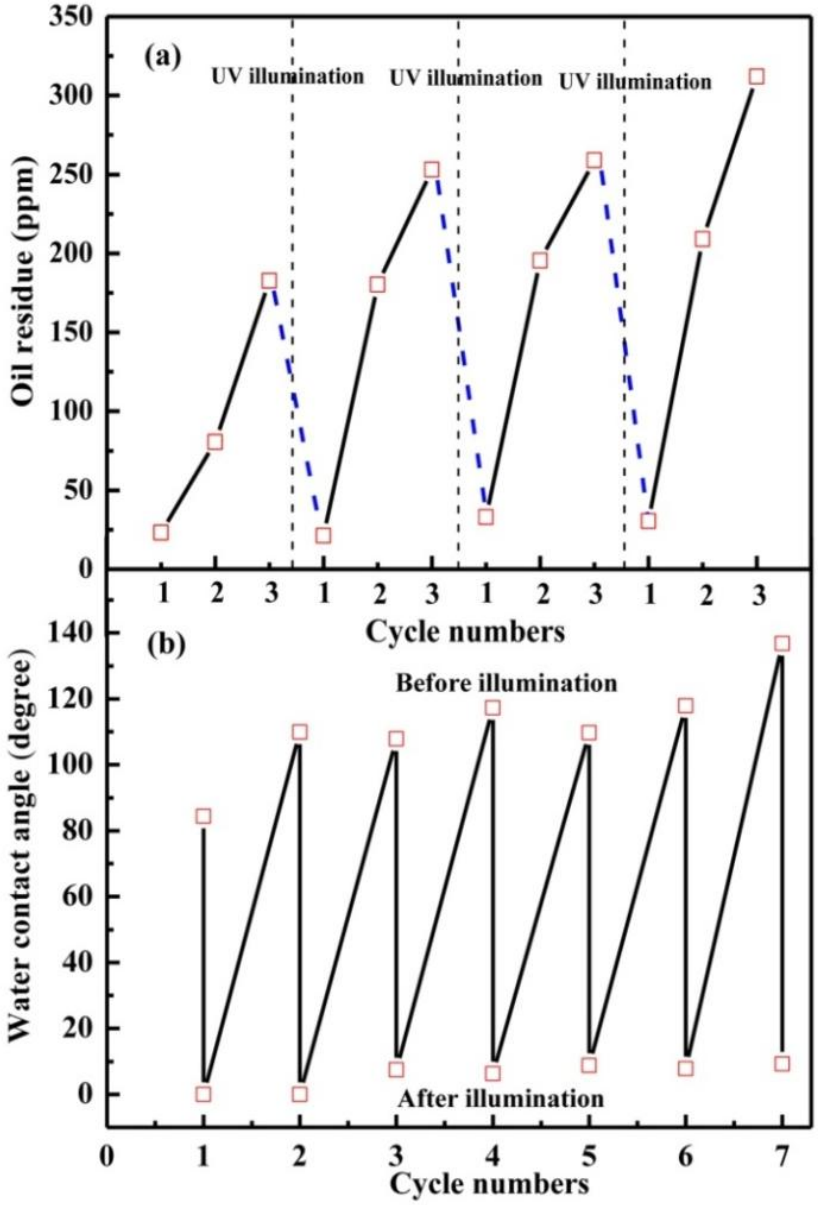

Figure 10

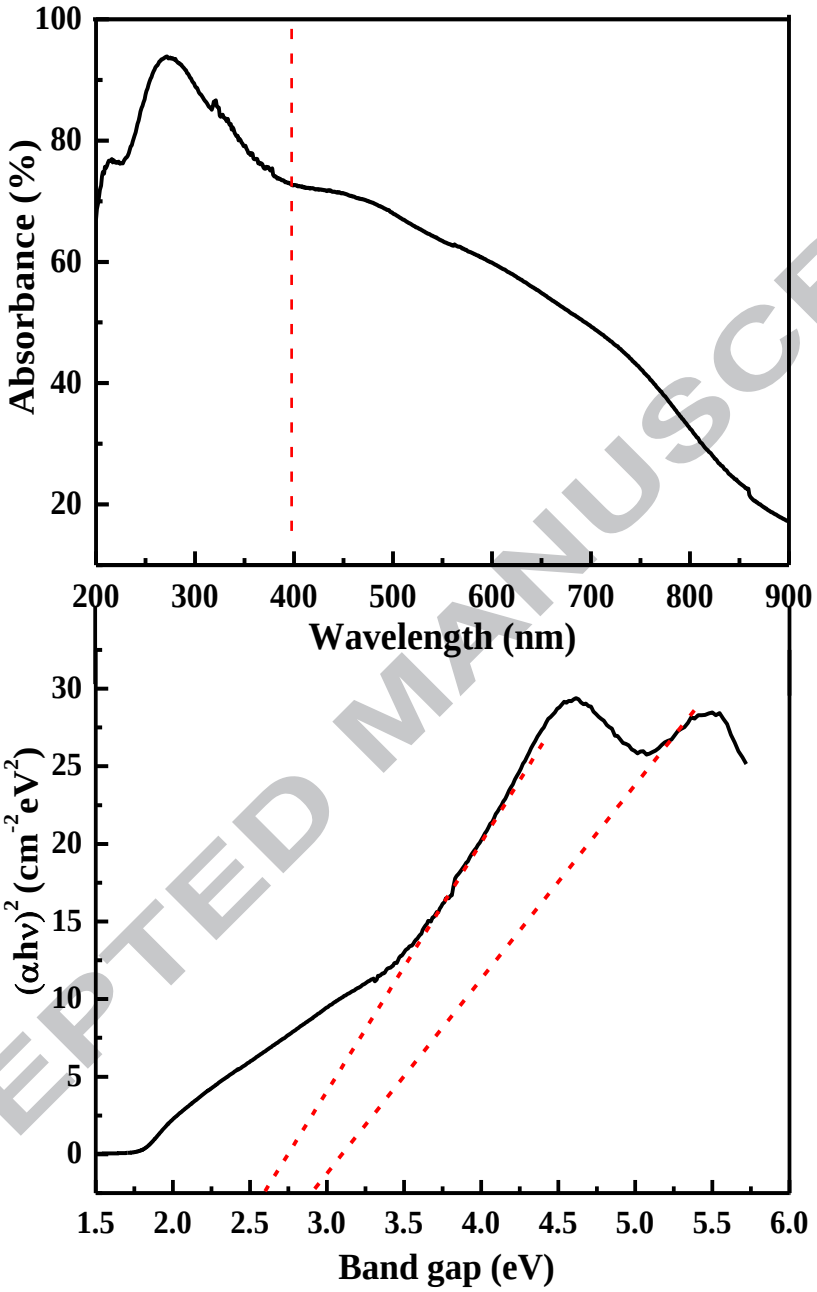

Figure 11

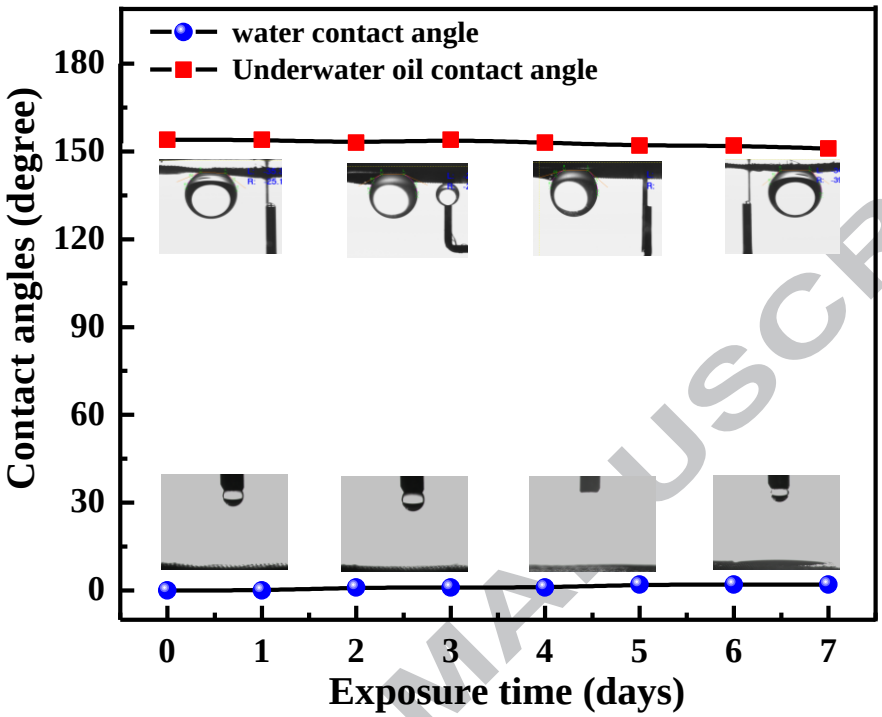

Figure 12

Graphical Abstract

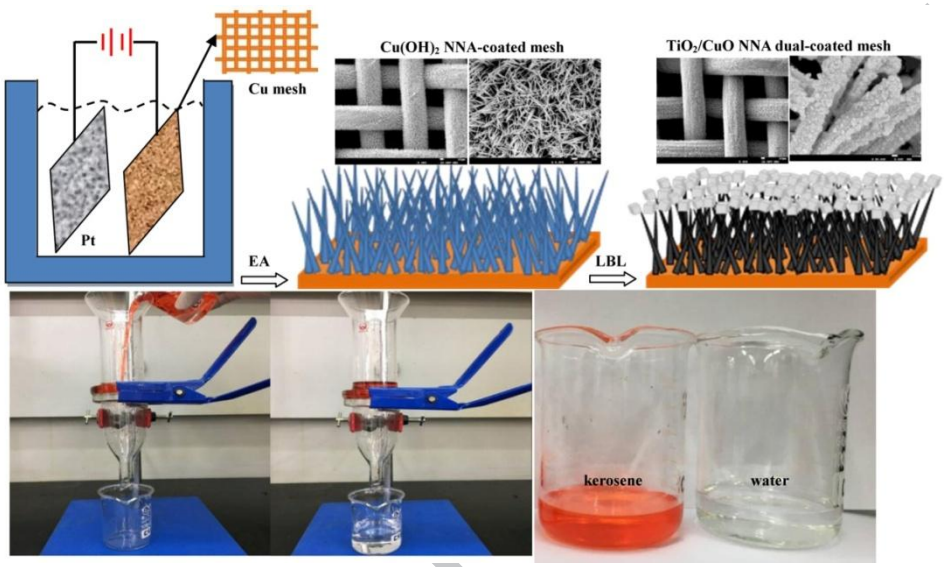

Highlights

• Well-ordered $Cu(OH)_2$ nanoneedle arrays (NNA) were grown on the copper mesh via anodization.

• Multilayer TiO_2 films were deposited on the CuO NNA-covered mesh via layer-by-layer self assembly.

• TiO_2/CuO dual-coated mesh displayed superhydrophlicity and underwater superoleophobic properties.

• .As-fabricated mesh was demonstrated a high separation efficiency and excellent water flux.

• As-fabricated mesh exhibited good self-cleaning ability under UV illumination for recycle use.